2012 IEEE International Conference on Robotics and Automation
RiverCentre, Saint Paul, Minnesota, USA
May 14-18, 2012

Characterizing the Stiffness of a Multi-Segment Flexible Arm During Motion

David Held, Yoram Yekutieli and Tamar Flash

Abstract— **A number of robotic studies have recently turned to biological inspiration in designing control schemes for flexible robots. Examples of such robots include continuous manipulators inspired by the octopus arm. However, the control strategies used by an octopus in moving its arms are still not fully understood. Starting from a dynamic model of an octopus arm and a given set of muscle activations, we develop a simulation technique to characterize the stiffness throughout a motion and at multiple points along the arm. By applying this technique to reaching and bending motions, we gain a number of insights that can help a control engineer design a biologically inspired impedance control scheme for a flexible robot arm. The framework developed is a general one that can be applied to any motion for any dynamic model. We also propose a theoretical analysis to efficiently estimate the stiffness analytically given a set of muscle activations. This analysis can be used to quickly evaluate the stiffness for new static configurations and dynamic movements.**

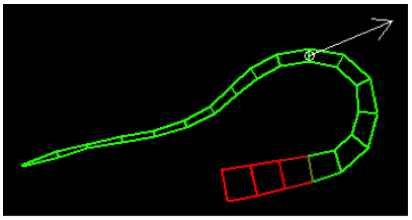

Fig. 1. Applying an external force at position = 0.095 m from the proximal end, with the arm configuration as it appears during a reaching movement at time t = 0.125 seconds. We are measuring the stiffness at the location marked by the white circle, located halfway between the nearby pair of dorsal and ventral muscles. The arrow shows one possible direction of the applied external force; in practice, we apply the force in 16 different directions through repeated simulation. Red segments represent a higher level of muscle activation; green segments represent a lower level of muscle activation.

I. INTRODUCTION

A number of recent robotics efforts have focused on developing flexible arms that are safer to interact with and can move around in small crowded spaces [1], [2]. Given the complexity of these high degree-of-freedom arms, some researchers have begun looking towards biological inspiration to develop control schemes for these arms [3]–[5]. One animal that has recently inspired new approaches in robotics is the octopus.

Octopuses are intelligent and dexterous animals known to be able to move efficiently under water and can perform complex tasks such as opening jars [6]. Previous work has suggested that octopuses are able to perform relatively complicated motions using simple control schemes [7]–[10]. By controlling the timing of muscle activation, the octopus is able to move its arms using a large repertoire of different movements.

Some work has begun on designing robots that can imitate octopus movements [1], [11], [12]. In order to fully understand octopus motion and replicate the control scheme, it is necessary to understand the motion in terms of impedance and particularly stiffness control. Given an octopus motion with known muscle activations determined through simulation and biological experiments, we aim to analyze the stiffness of the resulting motion.

A large number of techniques have been developed to measure endpoint stiffness during a multi-joint human arm movement [13]–[21]. However, all of these techniques have a number of limitations. First, these techniques require a subject that can perform repeated controlled experiments in a laboratory setting. These techniques are therefore not very conducive to measuring the stiffness of animal motions. Second, the measured stiffness typically combines reflexes with voluntary muscle activation and arm configuration, rather than separating these factors. Third, these techniques typically produce a single stiffness value for an entire movement at a single endpoint location, rather than showing how stiffness changes along an arm and throughout a movement. Last, these techniques are designed to evaluate the stiffness of pre-recorded movements and are less useful for predicting the stiffness of new movements, which may be necessary for robotic control applications.

Other approaches have attempted to predict endpoint stiffness [22]–[24] and have also derived joint stiffnesses. For a rigid arm, the relations between endpoint and joint stiffnesses are easier to determine, but for a highly flexible and nonlinear octopus arm [25], assessing the arm stiffness at different locations along the arm is a difficult task.

We make use of the multi-segment dynamical arm model described in [8], which is modeled after an octopus arm. By applying external perturbations in simulation, we evaluate the simulated deviation from the unperturbed trajectory. We use this trajectory deviation to compute the stiffness throughout the motion at different points along the arm.

Manuscript received September 16, 2011. This work was supported in part by the European Commission in the ICT-FET OCTOPUS Integrating Project, under contract #231608.

D. Held was with the Weizmann Institute of Science, Rehovot 76100 Israel. He is now with the Computer Science Department, Stanford University, Stanford, California 94305 USA davheld@cs.stanford.edu

Y. Yekutieli is with the Computer Science Department, Hadassah College, Jerusalem 91010, Israel yoramye@hadassah.ac.il

T. Flash is with the Department of Computer Science and Applied Math, Weizmann Institute of Science, Rehovot 76100 Israel tamar.flash@weizmann.ac.il

After explaining this technique and its theoretical motivations, we characterize the stiffness of reaching and bending movements. We then perform a theoretical approximation to analytically and efficiently estimate the stiffness given a set of muscle activations. The simulated stiffness values and the analytical stiffness estimates can be used to help understand the stiffness control strategies used by an octopus to perform various motions and to help roboticists develop control techniques that can imitate these motions.

II. BACKGROUND

A. Octopus Model

Although our stiffness analysis can be applied to any flexible arm model, we focus on applying it to the octopus arm model that is developed in [8]. This is a 2D dynamic segmented model based on physics experiments from a severed octopus arm. The octopus is a muscular hydrostat [25], so it maintains a constant volume throughout its motion. To enforce this constraint, the model is composed of 20 segments, each of which maintains a constant area through the use of a constraint force. The model also has drag forces, gravity, and spring forces. The model is composed of masses at the corners of each segment to which these forces are applied. The spring forces are modeled after the transverse and longitudinal muscles in an octopus arm and are controlled by the muscle activation, which is the control input to this dynamical system.

End-effector impedance is based on the manipulator Jacobian describing the geometric relationship between the joints, links, and endpoint position as well as the relationship between joint torques and end-point forces. However, because the octopus arm is a muscular hydrostat [25], the relationship between muscles lengths and forces and the endpoint position and force cannot be easily described using a simple geometric relationship. For example, contraction of the transverse muscles causes lengthening of the longitudinal muscles to preserve a constant volume. On the other hand, co-contraction of the longitudinal and transverse muscles might cause an increase in stiffness alone without a change in position. The model in [8] computes these constraint forces by determining the forces that would combine with the other model forces to maintain a constant volume for each segment. Thus while the octopus arm model in [8] behaves realistically, it does not directly give the net stiffness at the tip or at any point along the arm.

Additionally, both [8] and [26] analyze the muscle activations during a reaching motion of an octopus arm, while other motor tasks such as grasping [9] are less well understood. This paper analyzes the stiffness of both reaching and bending motions. By characterizing the motions using a stiffness representation, we can abstract away the details of the muscle activations and analyze the motions on a higher level that is more easily transferable to a robot model.

B. Theoretical Background

Burdet, et al. [27] have described a technique for measuring the arm stiffness field during a multi-joint human arm movement. Subjects were asked to perform a horizontal arm movement, during which an external force was exerted on the hand in randomly chosen directions. The stiffness K of the movement is computed by measuring the forces applied by the arm to an external apparatus and the amount of perturbation from the intended trajectory. The endpoint stiffness computed using this method is defined by

$$K\left(x,\dot{x},u\right) \equiv -\frac{dF_m}{dx} - \frac{dF_m}{du}\frac{\mathrm{du}}{dx} \tag{1}$$

where x is the position of the hand during the movement, F_m is the total endpoint force, and u represents the muscle activations for the movement. The first term on the right side of equation 1 represents the stiffness of the arm muscles for a given arm configuration during the movement. The second term represents the contribution to stiffness from reflexes, which causes a change in muscle activation, du, as the arm is perturbed by an amount dx. For an arm in simulation, it is difficult to model the reflex response of the octopus arm to an externally applied perturbation. Thus, we ignore the reflex term, and focus on estimating the contribution to stiffness of muscle activations and arm configuration.

We can then express the stiffness at a particular point x at time t as

$$K\left(x,t\right) = -\left(\lim_{x_{per}(t)\to x(t)} \frac{F_m\left(x_{per}\left(t\right)\right) - F_m\left(x\left(t\right)\right)}{x_{per}\left(t\right) - x\left(t\right)}\right) \tag{2}$$

where $x(t)$ is the unperturbed trajectory of the point and $x_{per}(t)$ is the perturbed trajectory. Although the stiffness computed using this method may be dependent on the inertia of the arm, it is a valid approximation for slow movements such as those executed underwater by an octopus arm. As the analysis in section VI will show, the method developed is relatively robust to changes in the magnitude of the control input for all points along the arm except for the segments nearest the tip. This implies that the approximation is valid for most of the arm for the domain being analyzed.

III. METHODS

The stiffness of the arm will vary throughout a movement as a function of the arm configuration and muscle activations. Additionally, the octopus arm does not have one specific endpoint, but rather can use any point along the arm as its effective endpoint for grasping. Thus we wish to evaluate the stiffness as a function of the position along the arm and as a function of time.

For a specific motion, the muscle activations that produce the motion are given by u(t). To calculate the stiffness at a given instant t_0, we simulate the arm for a short time interval I = [t_0, t_0+Δt] with a constant muscle activation u(t_0), starting from some initial arm configuration $x_{\mathrm{arm}}(t_0)$ and initial velocity $\dot{x}_{\mathrm{arm}}(t_0)$. The initial values are simply taken from the simulation at time t_0. Starting from this initial arm configuration and velocity, we run a short simulation for a small time interval I and record the unperturbed trajectory x(t) of some target point along the arm.

Next, an external force F_{ext} is applied to both the dorsal and ventral muscle masses near position l, our target location for measuring stiffness. The external force is applied at an angle $\theta = k\pi/8$, where $k = 0 \ldots 15$, in repeated simulation. An example is shown in Figure 1. With this external force applied, we again simulate the arm for a short time interval I, and compute the perturbed trajectory $x_{per}(t)$ of the point at position l on the arm. The unperturbed trajectory is then subtracted from perturbed trajectory as in equation 3, where the limit is approximated using a short time interval.

Throughout the simulated movement, we compute the total forces at the target position. We would ideally like to compute the stiffness as a continuous function of position along the arm. However, because we are using the segmented arm model of [8], we are limited to compute the stiffness at the discrete endpoints of each segment. Thus we calculate the stiffness at the midpoint between a pair of dorsal and ventral muscles (see Figure 1), computed as the average of the forces on the nearby dorsal and ventral masses.

The computed force is the vector sum of the static forces due to muscle activation $u(t_0)$, the gravitational force, and the static component of the constant volume constraint for the octopus arm [8]. We are only interested in the forces that contribute to stiffness, so we do not include internal or external damping forces in this calculation, nor do we include the dynamic component of the constant volume constraint force, as these forces contribute only to the arm damping but not to the arm stiffness. To separate the damping component of the motion from the stiffness component, we only include the static forces in our analysis. We can record the static components of these forces directly using our simulation, and we also do not need to consider the effect of exerting a force on an external apparatus, as in [27].

For a given arm configuration and muscle activation, we must compute a single 2x2 stiffness matrix that combines the forces and trajectories from applying the external force in different directions. We compute the stiffness matrix by solving for the least-squares solution to the following set of equations:

$$\begin{bmatrix} F_{static,x1} & F_{static,x2} & \cdots \\ F_{static,y1} & F_{static,y2} & \end{bmatrix} = K \vec{dx} = \begin{bmatrix} K_{xx} & K_{xy} \\ K_{yx} & K_{yy} \end{bmatrix} \begin{bmatrix} dx_1 & dx_2 & \cdots \\ dy_1 & dy_2 & \end{bmatrix}$$

where $dx = x_{per}(t) - x(t)$, and $dy = y_{per}(t) - y(t)$, for each of the 16 different angles of the external force.

The eigenvectors and eigenvalues of this stiffness matrix describe a stiffness ellipse, as explained in [28]. The major and minor axes of this ellipse are given by the eigenvalues of the stiffness matrix. The ellipse can further be characterized by its area, shape (the ratio of the eigenvalues), and the angle of its major axis. This information gives a rich description of how the magnitude and direction of stiffness change as a function of location on the octopus arm throughout a given motion.

IV. CHARACTERIZING STIFFNESS OF MOVEMENTS

A. Reaching

Using the above technique, we characterize the stiffness of a reaching movement [8] of the octopus arm. The arm is extended using a wave of muscle activation that propagates from the proximal end of the arm toward the distal end. The activation traveling time for this wave is 1 second, and each muscle is activated using an inverted sigmoid activation function.

At each point in time, and for every segment along the arm, the stiffness ellipses are computed, as described above. The shape and orientation of these ellipses can be visualized in Figure 2. As we will quantify below, the ellipses generally appear to be aligned with the tangential direction of the arm, with some deviation occurring around the bend point.

Fig. 2. Stiffness ellipses shown on the arm during a reaching movement. In order to fit all the stiffness ellipses of different magnitudes in this figure, the ellipses are all scaled to appear roughly the same size, but their shape and angle are still preserved. Note that the ellipses are generally aligned with the tangential direction of the arm, with some deviation occurring at the bend point, marked by the blue arrow. Red segments represent a higher level of muscle activation; green segments represent a lower level of muscle activation.

Shown in Figure 3, the size of the ellipse, defined by its area, roughly corresponds to the overall stiffness of the location on the arm. Proximal locations on the arm stiffen before distal locations, as the wave of muscle activation reaches each part of the arm.

One significant aspect of a reaching movement is the location of the bend point [7]. As the arm extends, the bend point is propagated distally. To estimate the position of the bend point, regions of high curvature are computed, defined by the locations on the arm where adjacent segments differ in orientation by more than 45 degrees. As can be seen in Figure 3, most of the stiffening occurs after the bend has passed a given segment [26].

On the other hand, the shape and orientation of the stiffness ellipse do change significantly at the bend point (see Figure 3). The ellipse gets elongated at the bend point, increasing the length of its major axis relative to its minor axis. Also, for most of the motion, the ellipse is located along the tangential direction of the arm. However, at the bend point the ellipse deviates from the tangential direction, instead pointing in an outward direction at an angle of about 30 degrees to the arm. Combined, these two effects allow the arm to advance forward during the reaching movement, despite the large perpendicular drag forces faced by the arm at the bend point.

As described above, in order to compute the stiffness matrix, a least-squares best fit approximation is made after

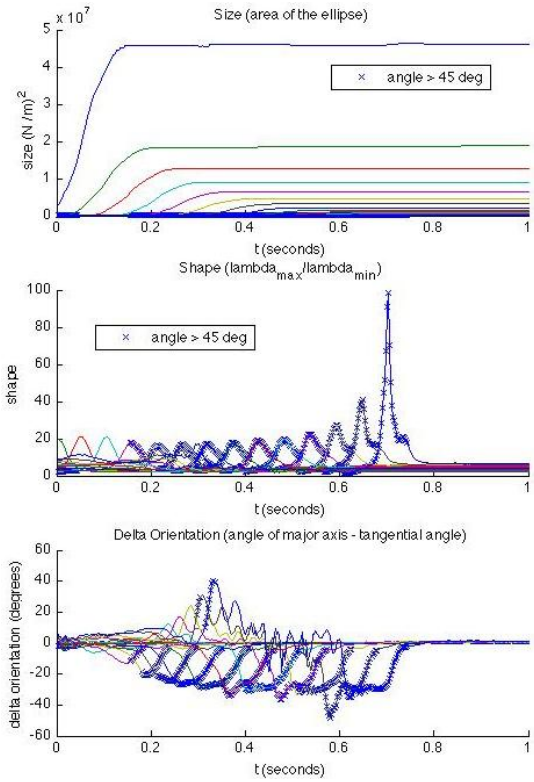

Fig. 3. The size, shape, and delta orientation of the stiffness ellipse throughout the reaching movement. Each colored curve corresponds to a different segment on the arm.

applying external forces to the arm in different directions. The error in this fit results in an error in the corresponding stiffness ellipse. For most of the movement, the error in the larger eigenvalue remains below 3.2% and the error in the smaller eigenvalue remains below 8%, with distal segments having more error than the proximal segments. This is probably due to the smaller mass and thinner size of the distal segments, resulting in more sensitivity to small perturbations.

At the bend location, the error increases significantly to 4.2% for the larger eigenvalues and 150% for the smaller eigenvalues. Because of the large error in computing the stiffness at the bend point, caution should be applied when drawing biological conclusions about the stiffness of an octopus arm near the bend point. On the other hand, the relatively low error throughout the rest of the arm indicates a higher confidence in our stiffness computations as a function of the arm configuration and muscle activations.

B. Bending

To measure the effect of bending on stiffness, we start from a straight arm with square segments, as opposed to the more realistic tapered arm that was used in the reaching movement. Using square segments creates symmetry and uniformity along the arm and helps isolate the effect of the bend angle on the stiffness. We apply differential ventral/dorsal activations to create a bend, as shown in Figure 4. The differential activation causes the dorsal muscles to contract more than the ventral muscles, bending the arm in the dorsal direction. The amount by which the arm bends is a function of the activation ratio between the dorsal and ventral muscles. In all simulations, the transverse muscles are activated to a level of 0.5, on a scale from 0 to 1.

Using the stiffness method described previously, we can compute the stiffness ellipses for the steady-state bend configuration, as shown in Figure 4. In each bend, the ellipses are all oriented tangential to the arm, and do not vary significantly in size and shape as a function of position along the arm. The variation in stiffness along the arm is consistently less than 0.6%, and increases slightly with an increasing bend angle.

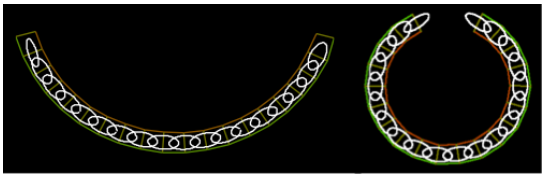

Fig. 4. Two bent arm configurations, with stiffness ellipses. The size of the ellipse is scaled for presentation purposes to fit on the figure. Red segments represent a higher level of muscle activation; green segments represent a lower level of muscle activation.

Figure 5 shows the size of the major and minor axes of the stiffness ellipse as a function of the bend angle, which closely align to the directions tangential and perpendicular to the arm, respectively. The deviation of the major axis of the ellipse from the tangential direction is shown at the bottom of Figure 6. As the bend angle of the arm increases, the arm becomes less stiff in the tangential direction and more stiff in the perpendicular direction. This can be understood by considering the contribution of neighboring segments to the stiffness. In a straight arm, the tangential components of the stiffness align in the same direction and thereby allow the arm to be especially stiff in the tangential direction but not as stiff in the perpendicular direction. In a bent arm, the change in orientation between neighboring segments reduces the tangential stiffness. At the same time, in a bent arm, the perpendicular component of the stiffnesses of neighboring elements aligns and increases the stiffness in the perpendicular direction.

As shown in Figure 6, the size of the stiffness ellipse decreases by 25% as the bend angle increases from 0 to 63 degrees. This decrease in stiffness is a result of the large decrease in the tangential stiffness as the bend angle increases, as explained above. This effect overcomes the small increase in perpendicular stiffness, resulting in an overall net decrease in stiffness as the bend angle increases.

The shape of the ellipse also changes as a function of the bend angle, becoming increasingly circular for larger bend angles. Figure 6 indicates that the ellipse is almost always oriented tangential to the arm. The only outliers occur at the extreme bend angles of 63 or -63 degrees; however, since the ellipses for this configuration are nearly circular, the orientation of the stiffness ellipse is not well defined for this configuration. Figure 6 confirms that the error bars

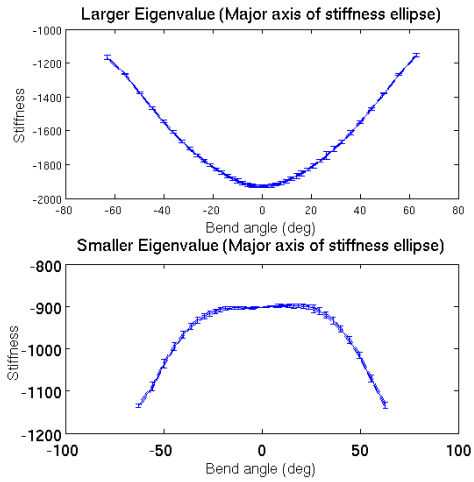

Fig. 5. Major and minor axes of the stiffness ellipse, as a function of bend angle. Error bars indicate variation in stiffness along the length of the arm for a given bend angle.

for the orientation at these extreme positions is very large, resulting from the symmetry of the nearly circular stiffness ellipse at these positions, while the error remains less than 4 degrees for bend angles smaller than 63 degrees.

V. THEORETICAL ANALYSIS

A. *Joint Stiffness*

For the segmented muscle model described in [8], the joint stiffness can be computed for a single segment. As a first approximation, let us assume that the segment is rectangular, with equal masses located at each of the corners, as shown in Figure 7. Let us further assume that the transverse muscles (marked by l_x) have equal activation, resulting in an equal stiffness of k_x determined from the muscle model (see [8]). Likewise, both longitudinal muscles have a stiffness of k_y. Due to the symmetry of the system, the two transverse muscles will thus remain at equal lengths, and the two longitudinal muscles will likewise remain equal.

We would like to analyze only the internal forces on this segment: the muscle force and the constraint force. We ignore the external gravity and drag forces in this section, as they do not contribute to the joint stiffness. Initially, let us assume that the springs have a rest length of 0. Note that, because all forces applied to the system are internal, the center of mass of the system will remain fixed, and the system will maintain the symmetries as shown.

As in section III, we can view the dorsal and ventral masses as a single mass group. The two masses on the right side of the segment are thus viewed as a single group of mass 2m. The position of the center of this group is given by

$$\vec{x} = \begin{bmatrix} l_x/2 \\ 0 \end{bmatrix}$$

with respect to the center of the segment. Using the analysis described in Appendix A, the dynamic equations for this mass group are given by

$$(2m)\,(\ddot{l_x}/2) = 2(-k_x l_x) + l_y p$$

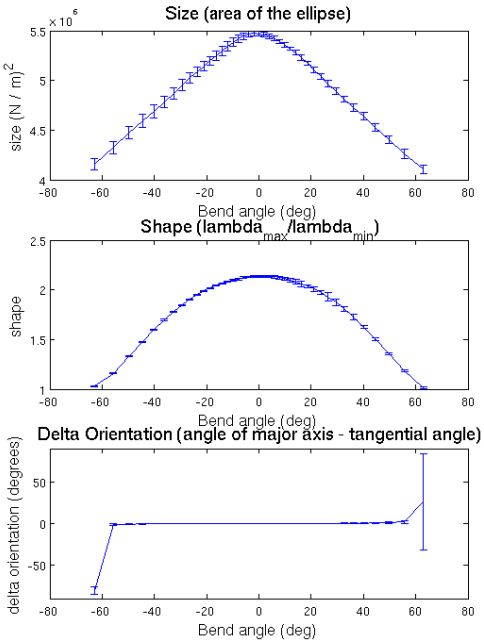

Fig. 6. Size, shape, and delta orientation of the stiffness ellipse, as a function of the bend angle. Error bars indicate variation in stiffness along the length of the arm, for a given bend angle.

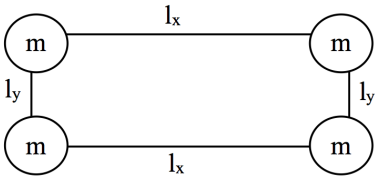

Fig. 7. Rectangular arm segment with equal masses at each corner

and the static internal force for this mass group is given by

$$F_{m_x} = \frac{2l_x(-k_x {l_x}^4 + k_y A^2)}{(A^2 + {l_x}^4)}$$

We can now compute the stiffness of this mass group with respect to the length of the segment as:

$$k_{xx} = -\frac{dF_{m_x}}{dl_x} = \frac{2[k_x {l_x}^8 + (5k_x + 3k_y)\,A^2 {l_x}^4 - k_y A^4]}{(A^2 + {l_x}^4)^2} \quad (3)$$

At the equilibrium position of $l_x = l_{x_{eq}}$, we get

$$k_{xx_{eq}} = \frac{8k_x k_y}{k_x + k_y} \quad (4)$$

One significant implication of this result is that the stiffness in the x-direction is symmetric with respect to k_x and k_y. Thus, at equilibrium, both k_x and k_y contribute equally to the stiffness of the segment. This can be understood by realizing that stretching the system in the x-direction simultaneously stretches the x side and compresses the y side of the segment, maintaining the constant area constraint. The

equilibrium position is thus the position at which these two restoring forces are equal, or

$$\frac{dF_{m_x}}{dl_x}=\frac{dF_{m_y}}{dl_y}$$

We can extend the above analysis, this time removing the simplifying assumption that the spring rest length is zero. Using the derivation from Appendix B, the dynamic equation for each mass in the x-direction is given by

$$m\ddot{l_x}=-2k_x(l_x-l_{x0})+l_yp \tag{5}$$

and the equilibrium stiffness is given by

$$k_{xx_{eq}}=\frac{2k_x{l_x}^4+4k_x\left(l_x-l_{x0}\right){l_x}^3+2k_yA^2}{A^2+{l_x}^4} \tag{6}$$

where l_{x0} is the rest length of the transverse muscles.

B. Comparing Theoretical Analysis to Simulation

In order to compare the computations of section V-A to the simulation results of section IV-A, imagine that the left end of a segment is held fixed, as shown in Figure 8.

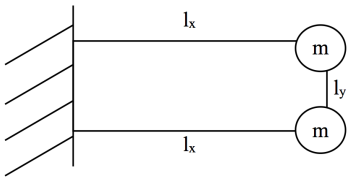

Fig. 8. Hypothetical arm segment with a fixed left end and a free right end

We can treat the dorsal and ventral masses as a 2m mass group whose center is located at $\vec{x}=\begin{bmatrix} l_x \\ 0 \end{bmatrix}$
In this case, the dynamic equations for this mass group are given by

$$(2m)\,\ddot{l_x}=-2k_x(l_x-l_{x0})+l_yp$$

Comparing this to equation 5, we see that the right side of both equations are identical, and thus the equilibrium stiffness for this mass group is also given by equation 6.

At the end of a reaching movement, the arm appears nearly linear, as shown in Figure 9.

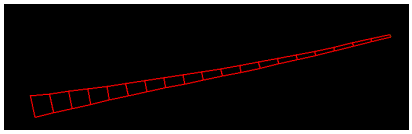

Fig. 9. Arm position at the end of a reaching movement

In this configuration, the arm can be modeled as a set of springs in series, as shown in Figure 10, approximating the stiffness at a point using only the estimated stiffness from the neighboring segments. On the distal end, the tip of the arm is not fixed, so we include only one neighboring distal segment in our model. Because we combine the ventral and dorsal masses when computing the stiffness, we model the point as a single mass of 2m.

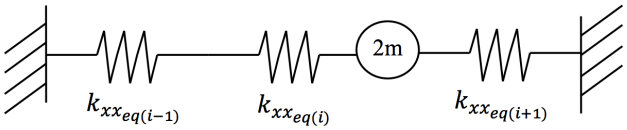

Fig. 10. A simplified arm model to estimate the stiffness of the arm

The equivalent stiffness using this model can now be computed by observing that the two proximal springs are in series, and both are in parallel with the distal spring, and thus:

$$k_{xx_{eq}}=\frac{1}{\frac{1}{k_{xx_{eq(i-1)}}}+\frac{1}{k_{xx_{eq(i)}}}}+k_{xx_{eq(i+1)}} \tag{7}$$

We can use this analytical formula to predict the tangential stiffness at any point on the arm, given the values for the individual muscle stiffnesses. The stiffness computed from this formula can be compared to the stiffness computed using a simulated motion, such as the reaching motion from section IV-A. This comparison is shown in Figure 11.

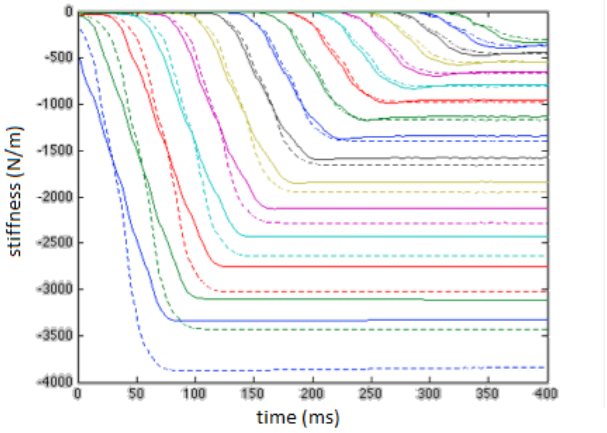

Fig. 11. Analytical stiffness prediction compared to stiffness evaluated from simulation

The analytical predictions agree well with the stiffnesses computed from the simulation. We can quantify the accuracy of this prediction by calculating the mean absolute percent error, relative to the stiffness computed using the full octopus arm simulation. The results are shown in Figure 12, using four analytical models of different complexity. The different models vary in whether to include a non-zero rest length for the muscles and whether we assume the segments to be at equilibrium. As can be seen from this figure, a non-zero rest length must be included to obtain an accurate model of the octopus arm. However, the figure also shows that we can assume that the segments are at equilibrium and still achieve roughly the same level of predictive accuracy.

VI. MODEL ROBUSTNESS

To test the robustness of the method, we analyze the effect of changing the external force on the tangential stiffness.

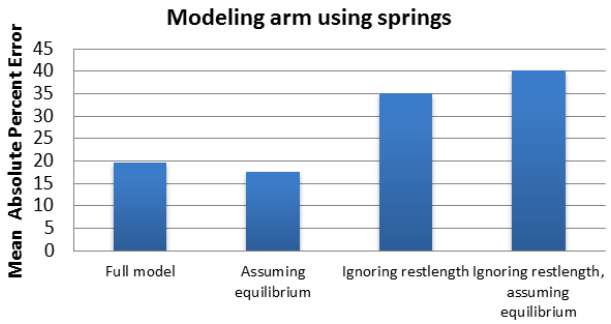

Fig. 12. Error in predicting the stiffness measured in simulation, using 4 different analytical models.

Using 0.01 N as the baseline, Figure 13 shows the effect of increasing the external force to 0.1 N. We see that, for the first 15 segments, the tangential stiffness changes by less than 1 percent as a result of this order of magnitude increase in the external force. For the last 5 segments, the computed tangential stiffness varies by up to 41% compared to the baseline. Thus, for a more precise calculation of the stiffness near the tip, a smaller external force should be applied in the simulation. However, for the purposes of this study to determine overall stiffness trends during different motions, this was not necessary.

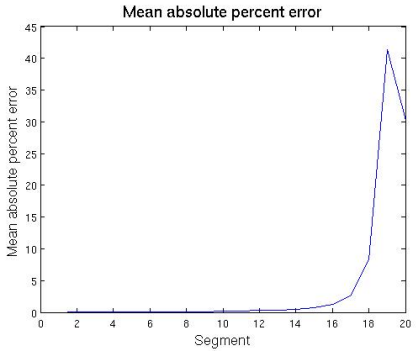

Fig. 13. Error in tangential stiffness as a function of segment number using an externally applied force of 0.1 N, compared to a baseline of 0.01 N. This evaluates the sensitivity of the stiffness calculation to the magnitude of the external force.

VII. CONCLUSIONS

By applying our novel method for estimating the stiffness from a dynamic model, we were able to obtain a number of unique insights about the octopus reaching and bending motions. This technique can be applied to analyze the stiffness of any motion using any dynamic model, and thus can be useful to engineers or biologists studying other animal or robot motions. The insights gained can be useful to control engineers designing biologically inspired impedance control methods. The analytic framework developed gives further insights into the underlying source of the stiffness values and how activation levels can be modified to produce a desired level of stiffness. We hope to further develop this analytic model to include rotational stiffness. We also hope to use the analytical stiffness as part of an impedance control system to control a simulated arm to follow new trajectories and stiffness values.

VIII. APPENDIX A

Similar to the procedure described in Appendix A of [8], we perform an analysis using Lagrangian mechanics, using the general coordinates $q = \begin{bmatrix} l_x \\ l_y \end{bmatrix}$ for the system. Each mass has a position of $\vec{x} = \begin{bmatrix} \pm l_x/2 \\ \pm l_y/2 \end{bmatrix}$, and the kinetic energy of this system is given by

$$T = 4\left(m(\dot{l_x}/2)^2\right) + 4\left(m(\dot{l_y}/2)^2\right)$$

and the potential energy is given by

$$V = 2(k_x {l_x}^2) + 2(k_y {l_y}^2) - p(l_x l_y - A)$$

where p is the pressure of the segment, and A is the constant area. We then get the following equations of motion for the system:

$$m\ddot{l_x} = -2k_x l_x + l_y p$$

$$m\ddot{l_y} = -2k_y l_y + l_x p$$

This can be written in matrix form as $M\ddot{q} = \vec{f_m} + Cp$, where $M = \begin{bmatrix} m & 0 \\ 0 & m \end{bmatrix}$, $\vec{f_m} = \begin{bmatrix} -2k_x l_x \\ -2k_y l_y \end{bmatrix}$, and $C = \begin{bmatrix} l_y \\ l_x \end{bmatrix}$. The constant area constraint for this segment is given by $l_x l_y$ = constant. Differentiating this equation twice, we get

$$\ddot{l_x} l_y + 2\dot{l_x}\dot{l_y} + l_x \ddot{l_y} = 0$$

or written in matrix form:

$$G\ddot{q} = \gamma$$

where G = $[l_y \;\; l_x]$ = C^T, and $\gamma = -2\dot{l_x}\dot{l_y}$. Continuing as in [8] and plugging in the appropriate values, we now get

$$p = \left(\frac{m}{{l_x}^2 + {l_y}^2}\right)\left[-2\dot{l_x}\dot{l_y} + \left(\frac{l_x l_y}{m}\right)(2k_x + 2k_y)\right] \quad (8)$$

Using this value in the dynamic equations, along with the substitution $l_y = A/l_x$ (based on the constant area constraint), we get the following dynamic equation:

$$m\ddot{l_x} = \frac{2l_x(-k_x {l_x}^4 + k_y A^2)}{A^2 + {l_x}^4} + \left(\frac{A^2}{A^2 + {l_x}^4}\right)\left(\frac{2m}{l_x}\dot{l_x}^2\right)$$

Note that the first term depends only on l_x and thus is a static, configuration-dependent term, whereas the second term is proportional to $\dot{l_x}^2$ and thus represents the internal damping caused by the constraint force.

At equilibrium, we have that $\dot{l_x} = \ddot{l_x} = 0$, $l_{x_{eq}} = \sqrt{A}\left(\frac{k_y}{k_x}\right)^{1/4}$, and $l_{y_{eq}} = \sqrt{A}\left(\frac{k_x}{k_y}\right)^{1/4}$. This defines the "rest-shape" for the segment. It is significant to note that this result agrees with the rest shape computed using the minimum potential energy approach of [29].

IX. Appendix B

Here we perform a stiffness analysis similar to that in Appendix A, but now with a non-zero rest length. The system potential energy is given by

$$V = 2(k_x(l_x - l_{x0})^2) + 2(k_y(l_y - l_{y0})^2) - p(l_x l_y - A).$$

Using this new value, the equations of motion for the system are given by

$$m\ddot{l_x} = -2k_x(l_x - l_{x0}) + l_y p$$
$$m\ddot{l_y} = -2k_y(l_y - l_{y0}) + l_x p$$

This time, the pressure force is given by

$$p = \left(\frac{m}{{l_x}^2 + {l_y}^2}\right)\left[-2\dot{l_x}\dot{l_y} + \frac{2k_x(l_x - l_{x0})l_y + 2k_y(l_y - l_{y0})l_x}{m}\right]$$

To find the equilibrium shape of the segment, we set $\dot{l_x} = \ddot{l_x} = 0$ as before, or

$$F_{m_x} = \frac{-2k_x(l_x - l_{x0}){l_x}^4 + 2k_y(A/l_x - l_{y0})A{l_x}^2)}{A^2 + {l_x}^4} = 0 \quad (9)$$

There is no simple analytical solution to this equation. Nonetheless, we can still compute that at equilibrium, the system settles into a shape such that

$$\frac{l_x(l_x - l_{x0})}{l_y(l_y - l_{y0})} = \frac{k_y}{k_x}$$

X. Acknowledgments

We would like to thank Avital Tsofe, Ido Zelman, and Ronit Fuchs for all of their help and advice.

References

[1] William Mcmahan, Bryan Jones, Ian Walker, Vilas Chitrakaran, Arjun Seshadri, and Darren Dawson. Robotic manipulators inspired by cephalopod limbs. In *Proc. CDEN Design Conf*, pages 1–10, 2004.

[2] Deepak Trivedi, Christopher D. Rahn, William M. Kier, and Ian D. Walker. Soft robotics: Biological inspiration, state of the art, and future research. *Applied Bionics and Biomechanics*, 5(3):99–117, 2008.

[3] P. Arena, C. Bonomo, L. Fortuna, M. Frasca, and S. Graziani. Design and control of an ipmc wormlike robot. *Systems, Man, and Cybernetics, Part B: Cybernetics, IEEE Transactions on*, 36(5):1044 –1052, oct. 2006.

[4] Auke Jan Ijspeert and Jérome Kodjabachian. Evolution and development of a central pattern generator for the swimming of a lamprey. *Artif. Life*, 5:247–269, June 1999.

[5] J. Jung, Y. Tak, B. Kim, J.-O. Park, S.-K. Lee, and J. Pak. Tadpole robot (tadrob) using ionic polymer metal composite (ipmc) actuator. In Y. Bar-Cohen, editor, *Society of Photo-Optical Instrumentation Engineers (SPIE) Conference Series*, volume 5051 of *Society of Photo-Optical Instrumentation Engineers (SPIE) Conference Series*, pages 272–280, July 2003.

[6] Graziano Fiorito, Christoph von Planta, and Pietro Scotto. Problem solving ability of octopus vulgaris lamarck (mollusca, cephalopoda). *Behavioral and Neural Biology*, 53(2):217 – 230, 1990.

[7] Yoram Gutfreund, Tamar Flash, Yosef Yarom, Graziano Fiorito, Idan Segev, and Binyamin Hochner. Organization of octopus arm movements: A model system for studying the control of flexible arms. *The Journal of Neuroscience*, 16(22):7297–7307, 1996.

[8] Yoram Yekutieli, Roni Sagiv-Zohar, Ranit Aharonov, Yaakov Engel, Binyamin Hochner, and Tamar Flash. Dynamic model of the octopus arm i. biomechanics of the octopus reaching movement. *Journal of Neurophysiology*, 94(2):1443–1458, 2005.

[9] German Sumbre, Graziano Fiorito, Tamar Flash, and Binyamin Hochner. Neurobiology: motor control of flexible octopus arms. *Nature*, 433:595–596, 2005.

[10] German Sumbre, Graziano Fiorito, Tamar Flash, and Binyamin Hochner. Octopuses use a human-like strategy to control precise point-to-point arm movements. *Current Biology*, 16(8):767 – 772, 2006.

[11] C Laschi, B Mazzolai, V Mattoli, M Cianchetti, and P Dario. Design of a biomimetic robotic octopus arm. *Bioinspiration & Biomimetics*, 4(1):015006, 2009.

[12] E. Guglielmino, N. Tsagarakis, and D.G. Caldwell. An octopus anatomy-inspired robotic arm. In *Intelligent Robots and Systems (IROS), 2010 IEEE/RSJ International Conference on*, pages 3091 – 3096, oct. 2010.

[13] David Franklin, Etienne Burdet, Rieko Osu, Mitsuo Kawato, and Theodore Milner. Functional significance of stiffness in adaptation of multijoint arm movements to stable and unstable dynamics. *Experimental Brain Research*, 151:145–157, 2003. 10.1007/s00221-003-1443-3.

[14] Rieko Osu, David W. Franklin, Hiroko Kato, Hiroaki Gomi, Kazuhisa Domen, Toshinori Yoshioka, and Mitsuo Kawato. Short- and long-term changes in joint co-contraction associated with motor learning as revealed from surface emg. *Journal of Neurophysiology*, 88(2):991–1004, 2002.

[15] Rieko Osu, Naoki Kamimura, Hiroshi Iwasaki, Eri Nakano, Chris M. Harris, Yasuhiro Wada, and Mitsuo Kawato. Optimal impedance control for task achievement in the presence of signal-dependent noise. *Journal of Neurophysiology*, 92(2):1199–1215, 2004.

[16] Rieko Osu, Etienne Burdet, David W. Franklin, Theodore E. Milner, and Mitsuo Kawato. Different mechanisms involved in adaptation to stable and unstable dynamics. *Journal of Neurophysiology*, 90(5):3255–3269, 2003.

[17] A. Kadiallah, G. Liaw, E. Burdet, M. Kawato, and D.W. Franklin. Impedance control is tuned to multiple directions of movement. In *Engineering in Medicine and Biology Society, 2008. EMBS 2008. 30th Annual International Conference of the IEEE*, pages 5358 –5361, aug. 2008.

[18] D. Bennett, J. Hollerbach, Y. Xu, and I. Hunter. Time-varying stiffness of human elbow joint during cyclic voluntary movement. *Experimental Brain Research*, 88:433–442, 1992. 10.1007/BF02259118.

[19] David J. Bennett. Torques generated at the human elbow joint in response to constant position errors imposed during voluntary movements. *Experimental Brain Research*, 95:488–498, 1993. 10.1007/BF00227142.

[20] Randy D. Trumbower, Matthew A. Krutky, Bing-Shiang Yang, and Eric J. Perreault. Use of self-selected postures to regulate multi-joint stiffness during unconstrained tasks. *PLoS ONE*, 4(5):e5411, 05 2009.

[21] Hiroaki Gomi and Mitsuo Kawato. Human arm stiffness and equilibrium-point trajectory during multi-joint movement. *Biological Cybernetics*, 76:163–171, 1997. 10.1007/s004220050329.

[22] David W. Franklin, Gary Liaw, Theodore E. Milner, Rieko Osu, Etienne Burdet, and Mitsuo Kawato. Endpoint stiffness of the arm is directionally tuned to instability in the environment. *The Journal of Neuroscience*, 27(29):7705–7716, 2007.

[23] K. P. Tee, E. Burdet, C. M. Chew, and T. E. Milner. A model of force and impedance in human arm movements. *Biological Cybernetics*, 90:368–375, 2004. 10.1007/s00422-004-0484-4.

[24] Masazumi Katayama and Mitsuo Kawato. Virtual trajectory and stiffness ellipse during multijoint arm movement predicted by neural inverse models. *Biological Cybernetics*, 69:353–362, 1993. 10.1007/BF01185407.

[25] William M. Kier and Kathleen K. Smith. Tongues, tentacles and trunks: the biomechanics of movement in muscular-hydrostats. *Zoological Journal of the Linnean Society*, 83(4):307–324, 1985.

[26] Yoram Yekutieli, Roni Sagiv-Zohar, Binyamin Hochner, and Tamar Flash. Dynamic model of the octopus arm. ii. control of reaching movements. *Journal of Neurophysiology*, 94(2):1459–1468, 2005.

[27] E. Burdet, R. Osu, D.W. Franklin, T. Yoshioka, T.E. Milner, and M. Kawato. A method for measuring endpoint stiffness during multi-joint arm movements. *Journal of Biomechanics*, 33(12):1705 – 1709, 2000.

[28] FA Mussa-Ivaldi, N Hogan, and E Bizzi. Neural, mechanical, and geometric factors subserving arm posture in humans. *The Journal of Neuroscience*, 5(10):2732–2743, 1985.

[29] Ilan Gendelman. Model-based control for an octopus arm. Master's thesis, The Weizmann Institute of Science, 2005.